Soft Matter

Cite this: *Soft Matter*, 2012, **8**, 2432

www.rsc.org/softmatter

PAPER

Three-dimensional complex-shaped photopolymerized microparticles at liquid crystal interfaces

Angel Martinez,[a] Taewoo Lee,[a] Theodor Asavei,[bc] Halina Rubinsztein-Dunlop[b] and Ivan I. Smalyukh*[ad]

Received 7th November 2011, Accepted 7th December 2011
DOI: 10.1039/c2sm07125h

Microparticles of arbitrary shapes immersed in the bulk of nematic fluids are known to produce dipolar or quadrupolar elastic distortions that can mediate long-range colloidal interactions. We use two-photon photopolymerization to obtain complex-shaped surface-bound microparticles that are then embedded into a nematic liquid crystal host with a uniform far-field director. By means of three-dimensional imaging with multi-photon excitation fluorescence polarizing microscopy, we demonstrate low-symmetry, long-range elastic distortions induced by the particles in the liquid crystal director field. These director distortions may provide a means for controlling elastic interactions in liquid crystals between custom-designed photopolymerized microparticles attached to confining solid substrates and nematic fluid-borne colloids, thus enabling elasticity-mediated templated self-assembly.

A beautiful analogy between the distortion of a nematic liquid crystal (NLC) around colloidal inclusions and the electric field created by point charges, dipoles, and quadrupoles allows for understanding many interesting experimental observations in the rapidly growing research field of NLC colloids.[1–20] NLCs are anisotropic fluids with the unique properties of long-range orientational ordering and elasticity that are typically associated with crystalline solids.[16,21,22] They comprise anisotropic building blocks, such as rod- or disk-shaped molecules, particles, or micelles, which tend to spontaneously orient themselves along a common direction $\boldsymbol{n}$, called "director." Unlike conventional fluids, nematics can transmit torques and induce elasticity-mediated forces that often cause relatively long-range interactions between particles, defects, and confining surfaces.[1,16] A number of factors, such as the molecular interactions at confining surfaces, presence of colloidal inclusions in the bulk or at surfaces of NLCs, chirality imposed by various chiral dopants (*i.e.*, dopants made of molecules that lack mirror symmetry), and application of external fields, can create continuous spatial variations of the molecular alignment and elastic distortions described by the spatially varying director field, $\boldsymbol{n}(\boldsymbol{r})$.[16] When introduced into a nematic fluid with a uniform far-field director $\boldsymbol{n}_0$, distortions of lower symmetry are expected to propagate to a longer distance.[16–20] This prediction was experimentally tested for both spherical and non-spherical colloidal particles in NLCs: the director distortions and ensuing elasticity-mediated interactions between dipolar colloids are longer ranged as compared to the case of quadrupolar colloids.[1–15]

In one of the readers' exercises of his book on *Physics of Liquid Crystals* (1st edition),[16] de Gennes considered a floating particle of an arbitrary shape in the NLC and argued that the particle will align in such a way that the elastic torque acting on it will vanish and that the monopole-like low-symmetry distortions (decreasing with distance d as $1/d$) can exist only when an external torque is acting on the particle. Although application of external forces and torques on particles can induce "elastic monopoles,"[16–20] they are unstable without external influence as the elastic torque exerted by the NLC medium causes anisotropic particles to equilibrate at an orientation with the lowest symmetry of distortions being dipolar with one or more dipole moments.[8] However, it is not clear whether interactions between surface-bound and NLC-borne particles follow a similar behavior. Furthermore, experimental demonstration of twisted director configurations induced by nanofabricated chiral structures in confined NLCs (see, for example, ref. 23) indicates the need for exploring how long-range elastic distortions can possibly be exerted by surface-bound low-symmetry micrometre- and nanometre-sized particles.

In this work, we have designed three-dimensional (3D) low-symmetry, surface-bound, photopolymerized particles to demonstrate that they can cause low-symmetry, long-range elastic distortions in $\boldsymbol{n}(\boldsymbol{r})$, which we probe by means of three-photon excitation fluorescence polarizing microscopy (3PEF-PM).[24,25] We demonstrate that these particles induce director twist and impose elastic torque on the NLC director field $\boldsymbol{n}(\boldsymbol{r})$ which is transmitted to an opposite confining surface of the liquid crystal cell. Our findings may enable novel means of

[a]*Department of Physics, Material Science and Engineering Program, Department of Electrical, Computer, & Energy Engineering, and Liquid Crystal Materials Research Center, University of Colorado, Boulder, CO, 80309, USA. E-mail: Ivan.Smalyukh@colorado.edu*
[b]*Quantum Science Laboratory, School of Mathematics and Physics, The University of Queensland, Brisbane, QLD, 4072, Australia*
[c]*School of Physics, Monash University, Clayton, Victoria, 3800, Australia*
[d]*Renewable and Sustainable Energy Institute, National Renewable Energy Laboratory and University of Colorado, Boulder, Colorado, 80309, USA*

patterning bulk alignment of NLCs and the design of novel long-range interactions between the NLC fluid-borne and surface-attached particles for their structured elasticity-mediated self-assembly.

A schematic diagram of a two-photon photopolymerization and 3PEF-PM setup is shown in Fig. 1a. A tunable (680–1080 nm) femtosecond Ti:sapphire laser (140 fs, 80 MHz, Chameleon Ultra-II, Coherent) is used as an excitation light source for both photopolymerization and 3PEF-PM (which is an imaging modality of nonlinear optical polarizing microscopy described in detail in references 24 and 25). For the two-photon photopolymerization, a femtosecond laser beam tuned to a wavelength of 780 nm is introduced into an inverted microscope (IX-81, Olympus) and tightly focused into a sample by an oil-immersion objective (100×, NA = 1.4). The exposure of the sample is controlled by a fast shutter (LS3Z2 obtained from Uniblitz, up to 200 Hz) introduced into the optical train of the photopolymerization setup immediately before the microscope (Fig. 1a). A computer-controlled XYZ nano-positioning stage (Nanocube P-611.3SF obtained from Physik Instrumente) changes the relative 3D position of the sample with respect to the focal point of the focused femtosecond laser beam with the precision of 0.2 nm. Laser beam intensity and its polarization direction at the sample plane are controlled by a half-wave plate and a Glan laser polarizer. To impose a computer-generated 3D-shape into the photocurable resin, we continuously translate the XYZ stage and time the shutter so that the focus of the femtosecond laser beam can visit and sequentially polymerize all points of the desired volume of the complex-shaped microparticle.

The cells used during the photopolymerization part of the sample preparation process consist of two coverslips, one of which is coated with a thin film of unidirectionally rubbed polyvinyl alcohol (PVA, obtained from Aldrich). The glass plates are spaced with two thin strips of parafilm. A small drop of UV-curable optical adhesive (NOA-61, obtained from Norland) is sandwiched between two coverslips held together by two pieces of Scotch tape. We then place the cell on a mounting clip attached to the Nanocube XYZ stage so that it can be scanned over the objective during the photopolymerization of 3D microparticles within the drop (Fig. 1c and d). In this process, the polymerization starts at the PVA–NOA interface and then advances away from the substrate as we shift the sample along the microscope's optical axis to "draw" the consecutive layers of the particle (Fig. 1b). After the photopolymerization of the desired surface-attached particles is completed, the cell is disassembled and the coverslip carrying the attached particles is lightly rinsed with acetone to wash away the excess, unpolymerized resin. Obtained particles can be kept surface-bound or released from the substrate by carefully poking with a needle (Fig. 1c and d).

The studied LC cells were constructed using one PVA-coated substrate having the polymerized particles bound to its surface and one substrate treated with polyimide (PI-2555, obtained from HD Microsystems) or derivative of methyl red (dMR). PVA and polyimide thin coatings were rubbed using velvet cloth to provide unidirectional planar surface anchoring. Prior to coating these substrates with dMR, PVA and PI-2555 alignment layers, we first cleaned the glass substrates using organic solvents and then additionally plasma-cleaned them for about 20 minutes. To obtain dMR coated substrates, we finally submerged the clean glass into the dilute dMR solution (<1 wt%) for 90 minutes, allowing the dMR molecules to chemically bond onto the glass surfaces. We then rinsed the substrates thoroughly with toluene to wash away any excess and unbound dMR, leaving only a molecular monolayer behind. The cell substrates were spaced with 15 μm spherical glass spacers mixed into epoxy glue. After

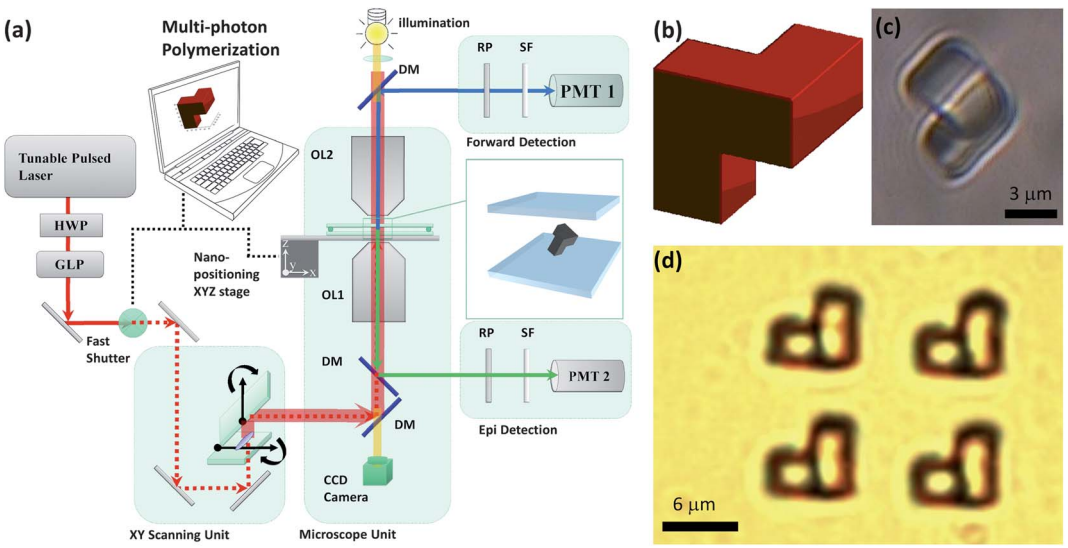

Fig. 1 Photopolymerization and nonlinear optical imaging by means of multi-photon excitation processes. (a) A schematic diagram of the multi-photon absorption photopolymerization and multi-photon excitation fluorescence microscopy setup. DM: dichroic mirror, GLP: Glan laser polarizer, HWP: half-wave plate, OL: objective lens, PMT: photo-multiplier tube, RP: rotating polarizer, and SF: selection filters. (b) A computer-generated model of the used low-symmetry microparticle. (c) A brightfield optical image of a microparticle obtained from the model shown in (b) by means of two-photon absorption photopolymerization. (d) A brightfield image of an array of four surface-bound photopolymerized microparticles having shape corresponding to the computer-generated model shown in (b).

the epoxy-spacer mix is cured, binding the glass plates together, we filled the cell with a room-temperature NLC, pentylcyanobiphenyl (5CB, obtained from Frinton Labs), and then sealed the edges with epoxy.

To study elastic interactions between colloids and the surface-bound photopolymerized particles, we have prepared an NLC colloidal dispersion of 2 μm spheres with vertical surface boundary conditions for $\boldsymbol{n}(\boldsymbol{r})$. We obtained these boundary conditions at the surface of particles by first dispersing the silica spheres in 5 wt% aqueous solution of the surfactant [3-(trimethoxysilyl)propyl]octadecyl-dimethylammonium chloride (DMOAP, purchased from Aldrich) and then sonicating for 30 minutes. The particles were then rinsed *via* sequential centrifugation at 3000 rotations per minute, replacement of the solvent with deionized water, and sonication for about 30 seconds. The rinsing process was repeated five times and the remaining water was then evaporated on a hot stage at about 120 °C for 10 hours. Once the particles were added to the NLC, the obtained dispersion was again sonicated for three hours to break colloidal aggregates and then used to fill in the cells immediately after the sonication.

3D imaging of the NLC was performed using 3PEF-PM. A femtosecond laser beam at the wavelength of 870 nm is introduced into the laser-scanning unit (FV-300, Olympus) and is focused into a sample using an oil-immersion objective (100×, NA = 1.4) of the inverted IX-81 microscope (Fig. 1a). A galvano-mirror pair in the scanning unit steers the position of a focused laser beam laterally within the focal plane of the objective while the motion of the objective along the microscope's optical axis is implemented by the use of a stepper motor. The 3PEF-PM signals are collected either by the same objective and detected in epi-detection mode with a photomultiplier tube (PMT2) or by another oil-immersion objective (60×, NA = 1.42) in a forward-detection mode with PMT1 (both tubes were obtained from Hamamatsu, model H5784-20). To control the linear polarization state of excitation light, we use a Glan laser polarizer. The laser beam at 870 nm wavelength excites the NLC molecules directly *via* the three-photon absorption process and the fluorescence light is then detected using a bandpass filter centered at 417 nm (bandwidth 60 nm). Since the excitation intensities required to induce significant three-photon absorption only exist in a small volume around the focus of the objective, this imaging approach yields an intrinsic 3D resolution. The fluorescence intensity in the 3PEF-PM with unpolarized fluorescence detection scales as $\sim\cos^6\theta$, where θ is the local angle between $\boldsymbol{n}(\boldsymbol{r})$ and the polarization of the excitation beam.[24,25] The polarized fluorescence textures allow us to reconstruct the 3D $\boldsymbol{n}(\boldsymbol{r})$. In addition to the 3PEF-PM imaging and photopolymerization, our setup (Fig. 1a) also allows for imaging using the conventional polarizing optical microscopy (POM) with and without inserted phase retardation plates.

NLC cells with one of the substrates coated with the photoresponsive dMR molecular monolayers allow for realization of both uniform and twisted configurations of $\boldsymbol{n}(\boldsymbol{r})$. Polarized illumination from a lamp source aligns the aromatic parts of dMR molecules perpendicular to the polarization direction. This allows one to set the boundary conditions for $\boldsymbol{n}(\boldsymbol{r})$ on this surface by continuously varying the easy axis orientation between parallel and perpendicular to the rubbing direction at the opposite PVA-coated substrates, *i.e.*, achieving either uniform (Fig. 2a and b) or twisted director structures (Fig. 2c and d). POM images with and without a phase retardation plate (Fig. 2a and b) suggest a complex low-symmetry configuration of $\boldsymbol{n}(\boldsymbol{r})$ around the surface-bound particle. The area near the particle is bright under crossed polarizers (Fig. 2a) and the structure of distortions and surrounding defects changes as one induces twist across the cell (Fig. 2c and d). Since the particle-induced structures are 3D in their nature and the spatial variation of the director field across the cell thickness is complex, reconstruction of the $\boldsymbol{n}(\boldsymbol{r})$ based on the POM images alone is difficult, although these images do indicate the presence of twist across the sample thickness in the regions of particles.

To get an insight into the 3D structure of $\boldsymbol{n}(\boldsymbol{r})$ induced by the photopolymerized particles, we perform the 3PEF-PM imaging. Using the near-infrared light excitation in 3PEF-PM allows us to mitigate the possible effects of imaging light on the dMR surface monolayer, which is sensitive to shorter-wavelength visible light. We also use excitation light of relatively low intensity to minimize its possible effects on dMR through the multiphoton absorption processes. The in-plane and vertical cross-section images obtained by 3PEF-PM are shown in Fig. 3a–c. Using these and other 3PEF-PM cross-sections, we construct the 3D model of $\boldsymbol{n}(\boldsymbol{r})$ around the particle schematically shown in Fig. 3e. The photopolymerized particle imposes tangential degenerate boundary conditions for the director at the NLC–particle interface. Within the sample with a uniform, in-plane, far-field

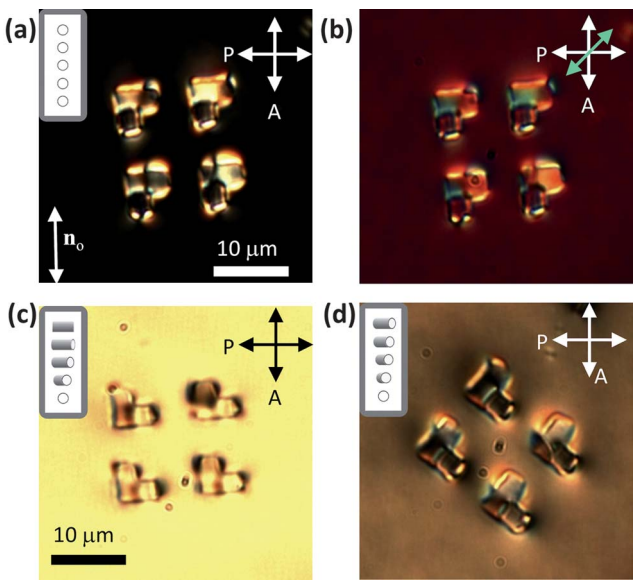

Fig. 2 Polarizing optical microscopy images of director structures around complex-shaped microparticles in uniform and twisted nematic LC cells. (a and b) POM images of a four-particle array in LC within a uniform far-field director $\boldsymbol{n}_0$ (a) between crossed polarizers and (b) with an additional phase retardation plate having the slow axis at 45 degrees with respect to the crossed polarizers, marked by the green double arrow. (c and d) POM images of the same array after the far-field director was twisted by (c) 90 degrees and (d) 45 degrees across the sample thickness *via* reorientation of dMR molecules in the monolayer as the sample cell was rotated by 90 degrees and 45 degrees, respectively. The NLC far-field molecular alignment across the sample thickness is shown in the insets of (a), (c) and (d).

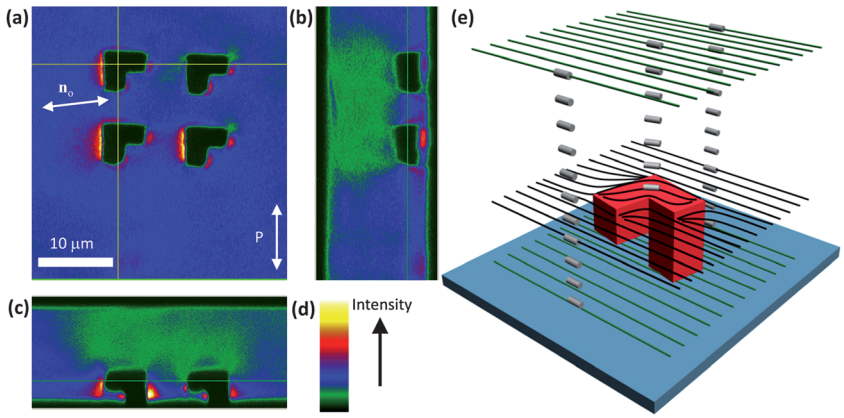

Fig. 3 3D director field around photopolymerized surface-bound low-symmetry microparticles. (a–c) Cross-sectional 3PEF-PM images of $\boldsymbol{n}(\boldsymbol{r})$ in the LC around the surface-attached microparticle obtained (a) in the plane parallel to confining substrates, (b and c) in the vertical cross-sections along two thin orthogonal lines shown in (a). (d) Color-coded fluorescence intensity scale used in (a–c). (e) 3D perspective of the reconstructed director field around the complex-shaped surface-bound colloidal microparticle; the green lines represent the surface boundary conditions for $\boldsymbol{n}(\boldsymbol{r})$ at the confining cell substrates and the black lines show $\boldsymbol{n}(\boldsymbol{r})$ in the plane coinciding with the top surface of the photopolymerized microparticle. The three columns of cylinders in (e) show that $\boldsymbol{n}(\boldsymbol{r})$ is twisted across the cell above the particle but is uniform far from it.

director $\boldsymbol{n}_0$, the substrate-bound particle is orientated so that all of its side faces are misaligned and at different angles with respect to $\boldsymbol{n}_0$. This, along with the shape of the top part of the particle, imposes strong elastic distortions of $\boldsymbol{n}(\boldsymbol{r})$ around the particle. We observe a twisted director structure propagating from the top surface of the particle toward the opposite dMR-coated glass substrate. Although the surface boundary conditions for $\boldsymbol{n}(\boldsymbol{r})$ at the NLC–particle interface are tangentially degenerate, the shape of the particle and the side faces lift this degeneracy so that $\boldsymbol{n}(\boldsymbol{r})$ in the central part of the top particle–NLC interface aligns roughly along a diagonal of the L-shaped top interface, as schematically shown in Fig. 3e. The twist distortion of $\boldsymbol{n}(\boldsymbol{r})$ then matches this average alignment of the director at the particle–NLC interface to the boundary conditions at the top substrate set by the optically controlled dMR monolayer (Fig. 3). Consistent with the results of 3PEF-PM imaging, the region above the particle appears bright in POM under crossed polarizers (Fig. 2a). Individual particles and their arrays (such as the 2×2 array shown in Fig. 2a) exhibit a similar behaviour and all induce twist of the same handedness, which is pre-determined by the symmetry and orientation of the used complex-shaped surface-bound particles (Fig. 2 and 3). Since the ensuing 3D structures of $\boldsymbol{n}(\boldsymbol{r})$ have all mirror symmetry planes broken and induce net twist with the helical axis along the normal to the substrates of the cell, this implies that the surface-bound photopolymerized particles in this geometry exert a torque on the NLC director. Experimental images indicate that $\boldsymbol{n}(\boldsymbol{r})$ at the NLC interface with the top dMR-coated substrate above the photopolymerized particle might slightly deviate (not shown in the schematic in Fig. 3e) from the easy axis set by polarized illumination, due to the fact that the surface anchoring at the dMR–NLC interface is finite (soft boundary conditions) and this deviation partially relieves the twist distortion in the NLC bulk above the particle (Fig. 3).

We have explored interactions of NLC-borne colloidal inclusions with the complex-shaped photopolymerized particles attached to the substrates. Despite the screening caused by the confinement, these elasticity-mediated interactions are long-range and strongly anisotropic. Fig. 4a shows an example of a trajectory of particle motion due to the elastic interaction between the floating colloid and a surface-bound particle. Both particles generate elastic distortions of $\boldsymbol{n}(\boldsymbol{r})$ in the NLC. The floating silica microsphere induces a hyperbolic point defect of charge $N = -1$, which compensates for the vertical boundary conditions, and the ensuing radial director structure around the particle surface (the radial director field is equivalent to a point defect of charge $N = 1$), as shown in Fig. 4d. These elastic distortions around the microsphere have a dipolar symmetry of $\boldsymbol{n}(\boldsymbol{r})$ while the distortions around the photopolymerized particle are monopole-like (since this surface-bound particle was intentionally fabricated to be oriented differently from what would be its equilibrium orientation in the NLC bulk). When the mobile particle is attracted toward the stationary one, the two particles share some of the induced elastic distortions and thus minimize the elastic energy cost due to the overall $\boldsymbol{n}(\boldsymbol{r})$ distortions in the cell. Although the elastic interactions are strongly screened by the proximity of confining substrates (especially the one to which the photopolymerized particle is bound) from which the floating dipolar colloidal particle repels,[26] the elastic binding energy of the mobile colloid to the stationary particle exceeds 1000 k_BT (Fig. 4c) and is comparable to the elastic binding energies between floating microparticles in the NLC bulk.[9] Furthermore, despite having physical underpinnings of elastic interactions similar to those studied for colloids in the NLC bulk, they may enable a qualitatively different type of medium-mediated templated self-assembly of particles using specially designed structured surfaces.

Elastic inter-particle interaction forces are characterized by the use of their balance with viscous forces, which are measured by video-tracking particle motion. We track the particle positions *vs.* time (Fig. 4a) and determine their velocity v. We neglect the inertia effects (since particle motion is overdamped and the Reynolds number is small) and determine the elastic force from its balance with the viscous drag force given by the Stokes' formula for a microsphere, $F_e = 6\pi\eta_{eff}Rv$ (Fig. 4b), where η_{eff} is the effective viscous drag coefficient for the particle with the

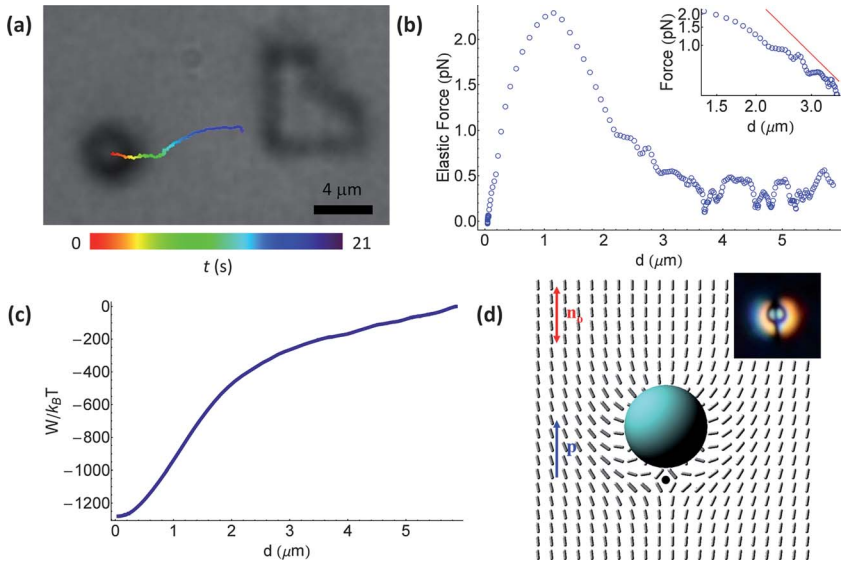

Fig. 4 Elasticity-mediated interaction between a surface-bound low-symmetry microparticle and a free-floating colloidal sphere with dipolar elastic distortions. (a) A brightfield microscopy frame from a movie showing a spherical particle at its initial position with an overlaid color-coded particle motion trajectory; the color-coded time scale is shown at the bottom of the image. (b) Elastic force exerted on the colloidal particle plotted as a function of the separation distance. The inset shows a log–log plot of this dependence over an intermediate range of distances; the red straight line shows a slope of −3. (c) The elastic interaction energy *vs.* separation distance. (d) Dipolar distortions of the director field around a spherical colloid embedded into the NLC with a uniform far-field director $\boldsymbol{n}_0$. The inset in (d) shows a POM image obtained between crossed polarizers parallel to the orthogonal image edges. The dipole moment of the elastic dipole shown in (d) is labeled by a blue arrow and "$\boldsymbol{p}$".

surrounding "corona" of $\boldsymbol{n}(\boldsymbol{r})$ distortions. η_{eff} depends on the motion direction of the particle with respect to $\boldsymbol{n}_0$ and also on the $\boldsymbol{n}(\boldsymbol{r})$ structure around the colloid. We use $\eta_{\text{eff}} = 86.4$ cP, as previously determined for a particle with dipolar $\boldsymbol{n}(\boldsymbol{r})$ in 5CB for a similar geometry.[27] We find that the maximum attractive elastic force is about 2.3 pN (Fig. 4b). This is an external force needed to separate the mobile colloid from the elastic trap produced by the surface-attached particle and, in analogy to the case of optical trapping, can be called "elastic trap escape force." Since the elastic force increases linearly (for small distances) as a function of the separation distance between the particle and its equilibrium location in the elastic trap, one can also determine the stiffness of this elastic trap, which is ~4.6 pN μm^{-1}. The elastic force decays rather weakly with distance to the final equilibrium location of the mobile dipolar colloid at the edge of the photopolymerized surface-bound particle (Fig. 4b). This might be due to the fact that the low-symmetry $\boldsymbol{n}(\boldsymbol{r})$ around the photopolymerized particle is monopole-like. In a bulk of an NLC, the interaction force between an elastic monopole (obtained, for example, by means of exerting an external torque on a non-spherical colloid) and an elastic dipole is expected to scale with center-to-center separation r_{cc} as $\propto r_{cc}^{-3}$. Indeed, the log–log plot in the inset of Fig. 4b shows that the elastic force between the NLC-borne and surface bound particles decays with distance weaker than what is expected for bulk dipole–dipole interactions ($\propto r_{cc}^{-4}$), although the slope changes from about −2 to about −3, depending on the range of distances. This is likely due to the fact that the observed elastic interactions are strongly screened by the effects of confinement, which weaken these interactions, especially at larger inter-particle distances (Fig. 4b).[28] Furthermore, at short distances, the dipole–monopole interaction is further modified by the trap-like behaviour with the NLC-borne mobile colloid coming to rest in the elastic trap generated by the surface-bound particle. New theories are needed for quantitative modelling of our experimental findings, since they cannot be fully explained within the frameworks of available theories for the elasticity-mediated interactions in the NLC bulk.

To conclude, we have demonstrated the feasibility of inducing monopole-like elastic distortions in NLCs by means of complex-shaped low-symmetry particles attached to the confining solid substrates of a liquid crystal cell and oriented differently from what would be their equilibrium orientation in the NLC bulk. This approach can be extended to particles with other surface boundary conditions, symmetry of distortions, chemical composition, *etc.* Furthermore, our findings may provide a means for the control of elastic interactions in NLCs between custom-designed particles attached to solid confining substrates and nematic fluid-borne colloids, thus enabling novel methods for templated self-assembly of colloidal superstructures.

This work was supported by the Renewable Sustainable Energy Initiative Seed Grant Program of the University of Colorado, International Institute for Complex Adaptive Matter (A.M. and I.I.S.), NSF grants DMR-0847782 (A.M., T.L., and I.I.S.), DMR-0820579 (A.M. and I.I.S.), HRD-0639653 (A.M.), and DMR-0844115 (A.M., T.L., and I.I.S.), and the Australian Research Council (T.A. and H.R.-D.). We thank Yue Shi and Dave Walba for providing dMR. We acknowledge discussions with V. Pergamenshchik, B. Senyuk, and M. Varney.

References

1 P. Poulin, H. Stark, T. C. Lubensky and D. A. Weitz, *Science*, 1997, **275**, 1170–1173.
2 U. Tkalec, M. Škarabot and I. Muševič, *Soft Matter*, 2008, **4**, 2402.
3 F. Brochard and P. G. de Gennes, *J. Phys. (Paris)*, 1970, **31**, 691.

4 T. C. Lubensky, D. Pettey, N. Currier and H. Stark, *Phys. Rev. E: Stat. Phys., Plasmas, Fluids, Relat. Interdiscip. Top.*, 1998, **57**, 610.
5 B. I. Lev, S. B. Chernyshuk, P. M. Tomchuk and H. Yokoyama, *Phys. Rev. E: Stat., Nonlinear, Soft Matter Phys.*, 2002, **65**, 021709.
6 I. Dierking, G. Biddulph and K. Matthews, *Phys. Rev. E: Stat., Nonlinear, Soft Matter Phys.*, 2006, **73**, 011702.
7 V. M. Pergamenshchik and V. A. Uzunova, *Condens. Matter Phys.*, 2010, **13**, 33602.
8 V. M. Pergamenshchik and V. A. Uzunova, *Phys. Rev. E: Stat., Nonlinear, Soft Matter Phys.*, 2011, **83**, 021701.
9 C. P. Lapointe, T. G. Mason and I. I. Smalyukh, *Science*, 2009, **326**, 1083–1086.
10 M. Škarabot and I. Muševič, *Soft Matter*, 2010, **6**, 5476–5481.
11 D. Engström, R. P. Trivedi, M. Persson, K. A. Bertness, M. Goksör and I. I. Smalyukh, *Soft Matter*, 2011, **7**, 6304–6312.
12 J. S. Evans, C. Beier and I. I. Smalyukh, *J. Appl. Phys.*, 2011, **110**, 033535.
13 Q. Liu, Y. Cui, D. Gardner, X. Li, S. He and I. I. Smalyukh, *Nano Lett.*, 2010, **10**, 1347.
14 I. I. Smalyukh, J. Butler, J. D. Shrout, M. R. Parsek and G. C. L. Wong, *Phys. Rev. E: Stat., Nonlinear, Soft Matter Phys.*, 2008, **78**, 030701(R).
15 G. M. Koenig, I.-H. Lin and N. L. Abbott, *Proc. Natl. Acad. Sci. U. S. A.*, 2010, **107**, 3998–4003.
16 P. G. de Gennes, *Physics of Liquid Crystals*, Oxford University Press, London, 1st edn, 1974.
17 V. M. Pergamenshchik and V. A. Uzunova, *Phys. Rev. E: Stat., Nonlinear, Soft Matter Phys.*, 2007, **76**, 011707.
18 B. I. Lev and P. M. Tomchuk, *Phys. Rev. E: Stat. Phys., Plasmas, Fluids, Relat. Interdiscip. Top.*, 1999, **59**, 591.
19 J.-I. Fukuda, B. I. Lev and H. Yokoyama, *J. Phys.: Condens. Matter*, 2003, **15**, 3841.
20 J. B. Fournier, *Eur. J. Phys.*, 1993, **14**, 184.
21 S. J. Woltman, D. G. Jay and G. P. Crawford, *Nat. Mater.*, 2007, **6**, 929–938.
22 P. M. Chaikin and T. C. Lubensky, *Principles of Condensed Matter Physics*, Cambridge Univ. Press, Cambridge, 2000.
23 K. Robbie, D. J. Broer and M. J. Brett, *Nature*, 1999, **399**, 764–766.
24 T. Lee, R. P. Trivedi and I. I. Smalyukh, *Opt. Lett.*, 2010, **35**, 3447–3449.
25 R. P. Trivedi, T. Lee, K. A. Bertness and I. I. Smalyukh, *Opt. Express*, 2010, **18**, 27658–27669.
26 A. Martinez, H. Mireles and I. I. Smalyukh, *Proc. Natl. Acad. Sci. U. S. A.*, 2011, DOI: 10.1073/pnas.1112849108.
27 H. Stark and D. Ventzki, *Phys. Rev. E: Stat., Nonlinear, Soft Matter Phys.*, 2001, **64**, 031711.
28 V. M. Pergamenshchik and V. A. Uzunova, *Phys. Rev. E: Stat., Nonlinear, Soft Matter Phys.*, 2009, **79**, 021704.